Vulnerability assessment of southern coastal areas of Iran to sea level rise: evaluation of climate change impact

Hamid Goharnejad*
Abolfazl Shamsai
Seyed Abbas Hosseini

Department of Civil Engineering,
Science and Research Branch,
Islamic Azad University, Tehran, Iran;

e-mail: Hgn1982@gmail.com

*corresponding author

e-mail: shamsai@sharif.edu
e-mail: abbas_hoseyni@srbiau.ac.ir

Abstract

Recent investigations have demonstrated global sea level rise as being due to climate change impact. Probable changes in sea level rise need to be evaluated so that appropriate adaptive strategies can be implemented. This study evaluates the impact of climate change on sea level rise along the Iranian south coast. Climatic data simulated by a GCM (General Circulation Model) named CGCM3 under two-climate change scenarios A1b and A2 are used to investigate the impact of climate change. Among the different variables simulated by this model, those of maximum correlation with sea level changes in the study region and least redundancy among themselves are selected for predicting sea level rise by using stepwise regression. Two Discrete Wavelet artificial Neural Network (DWNN) models and a Discrete Wavelet Adaptive Neuro-Fuzzy Inference System (DWANFIS) are developed to explore the relationship between selected climatic variables and sea level changes. In these models, wavelets are used to disaggregate the time series of input and output data into different components. ANFIS/ANN are then used to relate the

disaggregated components of predictors and predictand (sea level) to each other. The results show a significant rise in sea level in the study region under climate change impact, which should be incorporated into coastal area management.

1. Introduction

Recent investigations worldwide have demonstrated a global temperature (land and sea) increase of $0.76°C$ from 1850–1899 to 2001–2005 (IPCC 2007). This temperature increase is greater in the northern hemisphere. Global warming has significant effects on the living environment, which may result in changes to river flow patterns and sea levels. It is predicted that the global sea level rise by the end of the 21st century will be between 0.18 m and 0.4 m (Pfeffer et al. 2008). Analyses of tide gauge records and satellite altimetry in open oceans show that the range of sea level changes is different in various regions (Bindoff et al. 2007). Assessments of coastal zone vulnerability to sea level rise and the implementation of adaptation strategies are key issues in dealing with climate change impact. Projections of global sea level changes under probable climate change scenarios have shown that the risk of flooding is increasing over low-lying coastal regions (Houghton et al. 2001).

Recent applications of Artificial Intelligence (AI) techniques have demonstrated their great capability in dealing with stochastic time series such as sea levels. When the underlying physical relationships in time series are not fully understood, AI techniques can be effectively used for their simulation. Two of these models, widely used in recent decades, especially in the field of hydrological analyses and for prediction purposes, are artificial neural network (ANN) and neuro-fuzzy inference system (ANFIS) models (Salahshoor et al. 2010). ANNs have been widely and successfully used for hydrological modelling as well as prediction purposes because of their ability to discover patterns in data that cannot be explored by human researchers and conventional statistical methods (Masters 1993).

The use of the ANFIS model, a hybrid of the ANN and fuzzy systems, has gained considerable attention in recent years because it can provide the opportunity to benefit simultaneously from the advantages of both ANN and fuzzy systems (Rajaee et al. 2009). In spite of the great flexibility of ANN and ANFIS, the results of their application to predicting sea level rise are not very satisfactory, because signal fluctuations are highly non-stationary and the physical hydrological process operates at a high level of uncertainty. The pre-processing of input and/or output data before these are fed into the prediction model is therefore necessary (Cannas et al. 2006).

The wavelet theory is an appropriate choice for data pre-processing, especially when dealing with non-stationary time series (Adamowski 2008a,b).

The wavelet decomposes a non-stationary time series into different components. This feature provides an interpretation of the series structure and helps to extract significant information about its history using just a few coefficients. Lu (2002) applied the wavelet transform to decompose the inter-decadal/annual components of rainfall data in the rainy season. Xingang et al. (2003) used wavelet analysis to investigate the rainfall spectrum and its development over northern China in the rainy season. Coulibaly & Burn (2005) employed wavelet analysis to interpret temporal variability of annual Canadian stream flows and to explain the dynamic relationship between these stream flows and climate variability in the northern hemisphere. Partal & Küçük (2006) investigated the trends of annual total precipitation series all over Turkey using a discrete wavelet transform (DWT). Their results showed that the DWT components provide a good explanation of the trend in the precipitation time series. All these studies demonstrate the effectiveness of the wavelet transform for investigating irregularly distributed multi-scale features of climate elements in space and time. The wavelet-ANN hybrid provides an effective tool that is used in time series forecasting problems, such as shallow groundwater level and daily discharge forecasts (Wang & Ding 2003), drought prediction (Kim & Valdés 2003), rainfall prediction (Partal & Kisi 2007, Nourani et al. 2009), daily suspended sediment prediction (Partal & Cigizoglu 2008) and monthly river flow prediction (Anctil & Tape 2004, Kisi 2008).

The objective of this paper is to investigate the impact of climate change on future sea level variability over the southern coastline of Iran. For this purpose, the outputs of a GCM model named CGCM3 under two climate change scenarios A1b and A2, which show the most optimistic and most pessimistic climatic changes in the future, are used. A set of predictors which better represent the variations in sea level are selected for sea level rise simulation among the GCM outputs using the stepwise method. The combinations of ANN/ANFIS models and wavelet theory are used to explore the relationship between predictors and predictand (sea level) and to investigate the influence of global climate change on sea level changes. These results of sea level simulation in the future are effectively used to determine areas at risk of inundation. The introduction is followed by a description of the proposed methodology, after which the case study and the data under consideration are presented. Thereafter come the results of the study and the discussion. The paper ends with a summary and conclusion.

2. Methodology

Recent records of sea level in different places all over the world show the ascending trend of sea level changes due to the impact of climate

change. This increase will affect human life and economy in coastal areas, especially in flat regions with high flooding potential. Recent studies have demonstrated the correlation of sea level changes with climatic variables. This study aims to use climatic variables to evaluate the sea level rise along the southern coast of Iran in the next 100 years under different climate change scenarios. Two simulation approaches, which are a combination of Wavelet theory with Artificial Neural Network and ANFIS models, are considered for the sea level simulation. The structure of the proposed methodology for investigating sea level changes under climate change impacts is given in Figure 1. In this structure, following their preparation and standardization, data are transformed using selected wavelet functions so that they can be used more effectively in the simulation process. The transformed data are then used to train the ANN and ANFIS models for sea level simulation. The models developed in this step with ANN and ANFIS are named DWANN and DWANFIS respectively. Invert wavelet transformation and de-standardization are applied to the simulated values to obtain actual values of sea level simulations. The steps of the proposed methodology are explained in the following section based on Figure 1.

2.1. Data preparation

The first step in developing prediction models is data preparation and checking data accuracy and adequacy. Data missing from sea level time series were filled in based on neighbouring station data, using the inverse squared distance method as follows:

$$Y_x = \frac{\sum_{i=1}^{n} P_i \times W_i}{\sum_{i=1}^{n} W_i}, \tag{1}$$

where $W_i = \dfrac{1}{D_i^2}$ is the weight of station i used for filling the gaps in the data of station x, P_i is the recorded sea level at station i, D_i is the distance between stations i and x, and n is the number of stations used for filling gaps in the data of station x.

For checking data adequacy, the Hurst (1951) coefficient, which evaluates the sufficiency of the available length of data for forecasting a phenomenon, is employed. The Hurst coefficient (K) is formulated as follows:

$$K = \frac{\log\left(\frac{R}{\sigma}\right)}{\log\left(\frac{N}{2}\right)}, \tag{2}$$

where σ is the standard deviation of the data, N is the length of the data series and R is the difference between the maximum and minimum
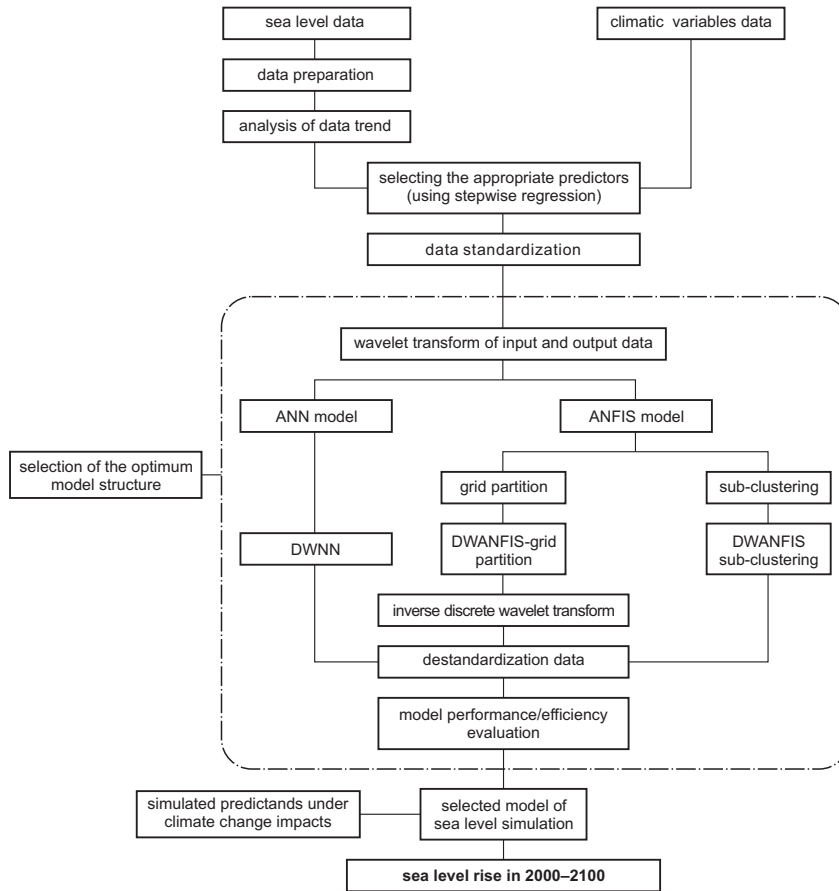
Figure 1. Structure of the proposed methodology for investigation of sea level changes under climate change impacts

cumulative difference from the average value in the data time series. Values of $K > 0.5$ show that the time series length is sufficient for prediction (Kleinow 2002).

2.2. Trend analysis

The Mann-Kendall test is a non-parametric test for identifying trends in time series data (Gilbert 1987). One benefit of this test is that the data need not conform to any particular distribution. The data values are evaluated as an ordered time series. Each data value is compared to all subsequent data values. The initial value of the Mann-Kendall statistic, S, is assumed to be 0 (i.e. no trend). If a data value from a later time period is higher than a data value from an earlier time period, S is incremented by 1. On the other hand, if the data value from a later time period is lower than

a data value sampled earlier, S is decremented by -1. The net result of all such increments and decrements yields the final value of S. Let x_1, x_2, $\ldots$ x_n, represent n data points, where x_j represents the data point at time j. Then, the Mann-Kendall statistic (S) is given by

$$S = \sum_{k=1}^{n-1} \sum_{j=k+1}^{n} \text{sign}(x_j - x_k), \tag{3}$$

where

$$\text{sign}(x_j - x_k) = \begin{cases} 1 & \text{if} & x_j - x_k > 0 \\ 0 & \text{if} & x_j - x_k = 0 \\ -1 & \text{if} & x_j - x_k < 0 \end{cases} \tag{4}$$

A very high positive value of S is an indicator of an increasing trend, and a very low negative value indicates a decreasing trend. However, it is necessary to compute the probability associated with S and the sample size, n, to statistically quantify the significance of the trend.

To calculate the associated probability, the variance of S, $\text{Var}(S)$, is calculated as follows:

$$\text{Var}(S) = \frac{n(n-1)(2n+5) - \sum_{p=1}^{g} t_p(t_p - 1)(2t_p + 5)}{18}, \tag{5}$$

where n is the number of data points, g is the number of tied groups (a tied group is a set of sample data having the same value) and t_p is the number of data points in the pth group. Then the normalized test statistic Z is calculated as follows:

$$Z = \begin{cases} \frac{S-1}{\text{Var}(S)} & \text{if} & S > 0 \\ 0 & \text{if} & S = 0 \\ \frac{S+1}{\text{Var}(S)} & \text{if} & S < 0 \end{cases} \tag{6}$$

The corresponding probability associated with Z is calculated based on the standard normal distribution with a mean of zero and a standard deviation of 1. The trend is decreasing when Z is negative and the probability level of significance (typically 95%) is less than the corresponding probability to S. When Z is positive and the corresponding probability of S is greater than the level of significance, the trend is increasing. Otherwise there is no significant trend.

2.3. Predictor selection

The correlation between the climatic signals and the sea level changes is investigated to determine the most appropriate predictors for sea level simulation. Even though some climatic signals are well correlated with sea level time series, they do not provide additional information for sea level analysis because they move together with other selected signals. Therefore, to select the more correlated signals and reduce the predictor's redundancy, stepwise regression is employed in this study.

Stepwise regression is a systematic method for adding and removing terms from a multilinear model based on their statistical significance in a regression. This procedure combines forward selection with backward elimination. The method begins with an initial model and then compares the explanatory power of incrementally larger and smaller models. If $\mathrm{SSR}_{l_1, \ldots, l_p}$ represents the sum of squares due to regression, when the p factors $X_{l_1}, \ldots, X_{l_p}$ are included in the multiple regression model, $\mathrm{SSR}_{l(p+1)|l_1, \ldots, l_p}$ will denote the increase in the regression sum of squares that comes about by adding factor $X_{l_{p+1}}$ as follows:

$$\mathrm{SSR}_{l_{(p+1)}}|_{l_1, \ldots, l_p} = \mathrm{SSR}_{l_1, \ldots, l_{p+1}} - \mathrm{SSR}_{l_1, \ldots, l_p}. \tag{7}$$

The model with less $\mathrm{SSR}_{l(p+1)|l_1, \ldots, l_p}$ is preferred. In stepwise regression, backward elimination was performed after every forward selection step to remove redundant variables from the model. At each step, a statistical measure such as the p-value is used to investigate the significance of change in the $\mathrm{SSR}_{l(p+1)|l_1, \ldots, l_p}$ value with and without a potential term. The forward regression and backward elimination steps are repeated until no further significance change can be made to the model (see Storch & Zwiers (2003) for more information on this topic). The significance of the results is checked through the p-value. The p-value is the probability of getting a correlation as large as the observed value by random chance, when the true correlation is zero.

2.4. Sea level simulation

In the next step, the sea level simulation models are developed. For this purpose two different hybrid simulation models are considered. The first model is a hybrid of wavelet theory and ANN named DWNN, and the second one is a hybrid of wavelet theory and ANFIS called DWANFIS. In these models wavelet theory is employed to decompose the input and output data into several smoother time series, after which the relations between decomposed inputs and outputs are explored using ANN/ANFIS.

2.4.1. Discrete Wavelet Theory

The wavelet transform was introduced at the beginning of the 1980s and has been widely used in different scientific fields. Labat (2005) has discussed the most recent contributions in wavelet applications. The time-scale wavelet transform of a continuous time signal, $x(t)$, is formulated (Mallat 1998):

$$W(a,b) = \frac{1}{\sqrt{a}} \int_{-\infty}^{+\infty} g^* \left(\frac{t-b}{a} \right) x(t) \, dt \, , \tag{8}$$

where * corresponds to the complex conjugate and $g(t)$ is called the wavelet function or mother wavelet. $T(a,b)$ is the wavelet coefficient, a is the model parameter and acts as a dilation factor, b is a temporal translation of the function $g(t)$, which allows the study of the signal around b.

In hydrologic cases where just one discrete time signal is available, equation (8) is discretized using the logarithmic uniform spacing for scale discretization with correspondingly coarser resolution of the b locations, which allows for N transform coefficients to completely describe a signal of length N.

The DWT of a signal x is calculated by passing it through a series of filters. First, the samples are passed through a low-pass filter with impulse response, resulting in a convolution of the two. At the same time, the signal is decomposed using a high-pass filter. The outputs give the detail coefficients (from the high-pass filter) and approximation coefficients (from the low-pass). The two filters are related to each other and they are known as a quadrature mirror filter. For a discrete time series, x_i, the dyadic wavelet transform becomes (Mallat 1998)

$$T_{m,n} = 2^{\frac{-m}{2}} \sum_{i=0}^{N-1} g(2^{-m} \, i - n) x_i \, , \tag{9}$$

where $T_{m,n}$ is the wavelet coefficient for a discrete wavelet of scale $a = 2^m$ and location $b = 2^m n$. Equation (9) considers a finite time series, x_i, $i = 0, 1, 2, \ldots, N-1$, and N is an integer power of 2: $N = 2^M$. This gives the ranges of m and n as $0 < n < 2^{-M} \, m - 1$ and $1 < m < M$ respectively. At the largest wavelet scale (i.e. 2^m where $m = M$) only one wavelet is required to cover the time interval, and only one coefficient is produced.

The total number of wavelet coefficients for a discrete time series of length $N = 2^M$ is then $1 + 2 + 4 = 8 = \ldots + 2^{M-1} = N - 1$. In addition, the signal smoothed component, $\overline{T}$, is left, which is the signal mean. Thus,

a time series of length N is broken into N components, i.e. with zero redundancy. The inverse discrete transform is given (Mallat 1998):

$$x_i = \overline{T}(t) + \sum_{m=1}^{M} W_m(t),\tag{10}$$

in which $\overline{T}(t)$ is called the approximation sub-signal at level M and $W_m(t)$ are detail sub-signals at levels $m = 1, 2, \ldots, M$. The wavelet coefficients, $W_m(t)$ $(m = 1, 2, \ldots, M)$, provide the detail signals, which can capture small features of interpretational value in the data; the residual term, $\overline{T}(t)$, represents the background information of data.

Because of the simplicity of $W_1(t)$, $W_2(t)$, $\ldots$, $W_M(t)$, $\overline{T}(t)$, some interesting characteristics, such as the period, hidden period, dependence and jump can be easily diagnosed through wavelet components.

In this study some irregular mother wavelets such as Haar, Db2 (Daubechies wavelet of order 2) and Coif1 were used; they are illustrated in Figure 2. Haar is the first and simplest wavelet. A Haar wavelet is discontinuous, and resembles a step function. A Daubechies wavelet has no explicit expression exception. However, the square modulus of the transfer function of T is explicit and fairly simple. Coiflets are discrete wavelets that have scaling functions with vanishing moments. The wavelets are near-symmetric; their functions have $N/3$ vanishing moments and scaling functions $N/3 - 1$ and have been used in many applications (see Mallat (1998) for more information).
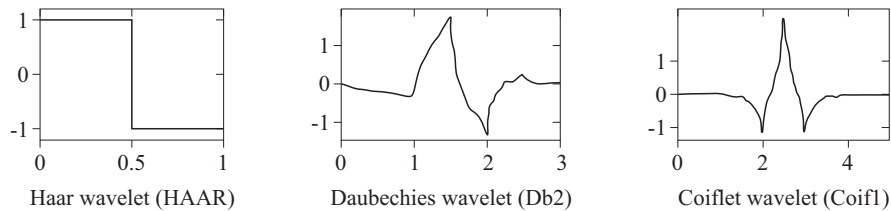
Figure 2. Profiles of the wavelet transformations considered in this paper (Mallat 1998)

2.4.2. Artificial Neural Networks

A feed forward neural network model or MLP, consisting of multiple layers of nodes in a directed graph, utilizes a supervised learning technique called back propagation for training the network. Mathematically an MLP can be written as

$$y = \varphi \left(\sum_{i=1}^{n} \omega_i r_i + b \right),\tag{11}$$

where ω_i is the weight corresponding to the input variable of r_i, b is the bias, φ is the activation function and n is number of input variables (Bishop 1995, Haykin 1998). For more information, see Rosenblatt (1961) and Rumelhart et al. (1986).

2.4.3. Discrete Wavelet artificial Neural Network

The DWNN model is a combination of the wavelet transform and ANN models. The DWNN can handle problems of larger dimension and it also has an efficient network structure in comparison with the ANN models:

$$y_{\text{DWNN}} = \varphi \left(\sum_{i=1}^{n} \omega_i \, T_{m,n} + b \right) , \qquad (12)$$

so

$$y_{\text{DWNN}} = \varphi \left(\sum_{i=1}^{n} \omega_i \left(2^{\frac{-m}{2}} \sum_{i=0}^{N-1} g(2^{-m}i - n)x_i + b \right) \right) . \qquad (13)$$

The model parameters are the same as in eqations (9) and (11). In the DWNN model the input variable r_i of the ANN model is replaced with the decomposed series, $T_{m,n}$, provided by the wavelet application. In equation (13) $T_{m,n}$ is replaced with its equivalent from equation (9). In this model the decomposed time series of selected climate signals through wavelet theory are used for training the ANN model. ANN models with different structures are developed and the model with the best performance is used for simulating sea level in the future under climate change impacts.

2.4.4. Adaptive Neuro-Fuzzy Inference System model

Neuro-fuzzy systems are fuzzy systems that employ ANN theory to determine their properties (fuzzy sets and fuzzy rules) by processing data samples. Neuro-fuzzy systems harness the power of two paradigms – fuzzy logic and ANNs – by utilizing the mathematical properties of ANNs for tuning rule-based fuzzy systems. A specific approach in neuro-fuzzy development is the adaptive neuro-fuzzy inference system (ANFIS), which has yielded significant results in modelling nonlinear functions (Maguire et al. 1998).

ANFIS uses a feed-forward network to search for fuzzy decision rules that perform well on a given task. Using a given input-output data set, ANFIS creates an FIS for which membership function parameters are adjusted using either a back propagation algorithm alone or a combination of a back propagation algorithm and a least-squares method. This factor allows the fuzzy systems to learn from the data being modelled.

A first-order Takagi-Sugeno fuzzy model with two inputs and one output is considered, so that for each input there are two membership functions. The entire system consists of five layers, and the relationship between the input and output of each layer is summarized as follows:

Layer 1: The output of the ith node in layer 1 is denoted as $O_{1,\,i}$ defined by:

$$
\begin{cases}
O_{1,\,i} = \mu_{A_i}(x) & for \quad i = 1,\,2 \\
O_{1,i} = \mu_{B_{i-2}}(y) & for \quad i = 3,\,4
\end{cases}
,
\tag{14}
$$

where $\mu_{A_i}(x), \mu_{B_{i-2}}(y)$ can adopt any fuzzy membership function. For example, if the bell-shaped membership function is employed, $\mu_{A_i}(x)$ is given by

$$
\mu_{A_i}(x) = \frac{1}{1 + \left\{ \left(\frac{x - c_i}{a_i} \right)^2 \right\}^{b_i}},
\tag{15}
$$

where a_i, b_i and c_i are the parameters of the membership function, governing the bell shaped functions accordingly.

Layer 2: Every node in this layer is a fixed node labelled G, which multiplies the incoming signals and output product. For instance,

$$
O_{2,\,i} = w_i = \mu_{A_i}(x) \times \mu_{B_i}(y), \quad i = 1,\,2.
\tag{16}
$$

Each output node represents the firing strength of a rule.

Layer 3: Every node in this layer is a circular node labelled N. The ith i node calculates the ratio of the ith rule's firing strength to the sum of all the rules' firing strengths. The output of this layer is called the normalized firing strength.

$$
O_{3,\,i} = \overline{w} = \frac{w_i}{w_1 + w_2}, \quad i = 1,\,2.
\tag{17}
$$

Layer 4: Node i in this layer computes the contribution of the ith rule towards the model output, with the following node functions:

$$
O_{4,\,i} = \overline{w_i} f_i = \overline{w_i}(p_i x + q_i y + r_i),
\tag{18}
$$

where $w_i w$ is the output of layer 3 and $\{p_i, q_i, r_i\}$ is the parameter set. Parameters in this layer are referred to as consequent parameters.

Layer 5: The single node in this layer is a fixed node labelled P that computes the overall output as the summation of all incoming signals.

$$\text{OverallOutput} = O_{5,i} = \sum_i \overline{w_i} f_i = \frac{\sum_i w_i f_i}{\sum_i w_i} . \tag{19}$$

ANFIS supports two different methods for antecedent membership function identification: grid partition (GP) (Jang 1993) and subtractive clustering (SC) (Chiu 1994). The grid partition method divides the data into rectangular subspaces based on a pre-defined number of membership functions and their types, producing rule base explosion. In contrast, the subtractive clustering method determines data point clusters by measuring their potential in feature space. This method has the advantage of avoiding the explosion of the developed rule base, a problem known as the 'curse of dimensionality'. When there are a few input variables, grid partition is a suitable method for data classification.

2.4.5. Discrete Wavelet Adaptive Neuro-Fuzzy Inference System

DWANFIS combines the abilities of DWT in feature extraction and selection with the characteristic decision capabilities of ANFIS techniques (Long & Datta 1996). DWANFIS is constructed based on the DWT theory (Ha et al. 2005). DWT allows one to decompose $x(t)$ using a wavelet function $g : R^n \rightarrow R$. Based on wavelet decomposition, the DWANFIS structure is formulated as follows:

$$y(x) = \frac{\sum_i^n w_i f_i(g(D_i(x - t_i))}{\sum_i^n w_i} , \tag{20}$$

where w_i are the weights of the DWANFIS inputs, t_i are translation vectors, D_i represents the dilation vectors, g is the wavelet function or mother wavelet, and f_i are Sugeno output functions of the ANFIS. The performance of these models is the same as DWANN (Barford et al. 1992, Mittal & Aadaleesan 2010).

2.5. Model performance evaluation indices

Different measures are available for evaluating the performance of the proposed sea level simulation models. In this study the Mean Squared Error (MSE), Root Mean Squared Error (RMSE), correlation coefficient (R) and Nash-Sutcliff coefficient (R^2_{NS}) indices are employed. These indices are formulated as follows:

$$\text{MSE} = \frac{\sum_{i=1}^N (S_i - O_i)^2}{N} , \tag{21}$$

$$\mathrm{RMSE} = \left[\frac{\sum_{i=1}^{N}(S_i - O_i)^2}{N} \right]^{0.5}, \tag{22}$$

$$R = \frac{N \sum_{i=1}^{N} S_i\, O_i - \sum_{i=1}^{N} S_i\, \sum_{i=1}^{N} O_i}{\left\{ \left[N \sum_{i=1}^{N} S_i^2 - \left(\sum_{i=1}^{N} S_i \right)^2 \right] \left[N \sum_{i=1}^{N} O_i^2 - \left(\sum_{i=1}^{N} O_i \right)^2 \right] \right\}^{0.5}}, \tag{23}$$

$$R_{\mathrm{NS}}^2 = 1 - \frac{\sum_{i=1}^{N}(S_i - O_i)^2}{\sum_{i=1}^{N}(O_i - \overline{O_i})^2}, \tag{24}$$

where O_i is the observed value at the ith time step, S_i is a forecast value at the same moment of time, N is the number of time steps and $\overline{O_i}$ is the mean value of the observed data. The higher values of the correlation coefficient show better model performance. In general, correlation coefficients > 0.7 provide satisfactory simulations (Makarynskyy et al. 2004). The RMSE and MSE are used to measure forecast accuracy, which increases from zero for perfect forecasts through large positive values as the discrepancies between forecasts and observations become increasingly large. The value of R_{NS}^2 decreases from 1 for a perfect forecast through large negative values for unreliable forecasts. In general, the negative values of R_{NS}^2 show unacceptable prediction results. Obviously, values of R_{NS}^2 closer to one and a small RMSE indicate the model's greater efficiency (Nourani et al. 2011).

2.6. Study area

The southern coastline of Iran, which is adjacent to the Persian Gulf and the Oman Sea, is the study area of this paper. With an area of $251\,000$ km^2, the Persian Gulf is connected to the Sea of Oman in the east, and its western end is marked by the major river delta of the Arvandrood, which carries the waters of the Rivers Euphrates and Tigris. The waters are overall very shallow, with a maximum depth of 90 m and an average depth of 50 m. The Sea of Oman, a strait (and not an actual gulf) connecting the Arabian Sea with the Persian Gulf, is a semi-enclosed basin with depths ranging from 100 to 3000 m. The climate in this region is more or less similar to that of the Indian Ocean.

The Iranian Tide Gauge Network, operated by the National Cartographic Centre (NCC), records the tidal elevations at 9 locations along the Persian Gulf and the Sea of Oman. Just four of these tide gauge stations have been used in this study, as they supply sufficient data for our purposes. Nevertheless, to increase the accuracy of the analyses, the Karachi station (southern Pakistan), located in the eastern part of the Sea

of Oman, is also included in this study. The locations of these stations and their characteristics are given in Figure 3 and Table 1 respectively.

Figure 3. Location of the tide gauges along the southern coast of Iran (http: //earth.google.com)

Table 1. Characteristics of the tide gauges on the southern coast of Iran (end of data series for all stations, 2008)

Station	Latitude [°N]	Longitude [°E]	Establishment [Year]	Mean [mm]	Standard deviation [mm]
Imam Hassan	29.83	50.25	1990	1862.14	159.37
Shahid Rajaie	27.10	57.07	1989	3242.57	78.62
Chabahar Port	25.28	60.62	1990	2758.62	415.67
Kangan	27.83	52.55	1989	2160.23	96.35
Karachi, Manora Island	24.80	66.97	1979	1771.25	114.38

For an evaluation of climate change impacts, the outputs of CGCM3 (3rd version of the coupled Canadian global climate model) under different climate change scenarios are used. The simulated monthly data of this model are accessible at http://loki.qc.ec.gc.ca/DAI. The surface grid representation of CGCM3 is about $3.75° \times 3.75°$ and includes 32 vertical grid levels, extending to 50 km above the surface.

3. Results and discussion

3.1. Data preparation

After the data gaps in the sea level time series have been filled, the Hurst coefficient is calculated for the five stations (see Table 2). Since the Hurst

coefficient for all of the tide gauges is more than 0.5, we can infer that the length of the sea level time series at all stations is sufficient to be considered for sea level change analysis.

Table 2. Results of Hurst coefficient analysis for the available tide gauge data

Row	Station	Hurst coefficient
1	Imam Hassan	0.502
2	Kangan	0.514
3	Shahid Rajaie	0.519
4	Chabahar	0.593
5	Karachi	0.534

The presence of a trend in the sea level records at each station is investigated using the Mann-Kendall method. The direction of Z indicates the direction of the trend. A positive (or negative) value of Z indicates an upward (or downward) trend. The critical value of Z at the 0.05 significance level of the trend test applied in this study is ± 1.96. The results of the trend analysis (Table 3) show that there is no significant trend at the different gauges, except at Karachi, which shows a slightly increasing trend. It should be noted that because of the characteristics of the wavelet transform, this method can deal with trending time series.

Table 3. Results of trend analysis for sea level data on the southern coast of Iran

Row	Station	Trend [mm year^{-1}]	Z	Z critical	Interpretation
1	Imam Hassan	15	1.09	1.96	no trend
2	Kangan	-1	0.00	1.96	no trend
3	Shahid Rajaie	-3	-0.16	1.96	no trend
4	Chabahar	1	0.00	1.96	no trend
5	Karachi	29	2.18	1.96	increasing

3.2. Predictor selection

The stepwise regression method is utilized to select the most appropriate predictors of sea level change (for results – see Table 4). The climatic variables with higher coefficients of determination and SSE and smaller P-values are selected as predictors of sea level changes along the Iranian south coast. The climatic variables of Sea Level Pressure (SLP), Geopotential Height (GH), Sea Surface Temperature (SST) and Sea Precipitable Water

Table 4. Results of stepwise regression application to CGCM3 outputs for a selection of sea level change predictors on the southern coast of Iran

No.	Predictor	P-value	R	MSE	Status
1	geopotential height (500 hPa)	0.0222	0.68	1.72	select
2	geopotential height (850 hPa)	0.1021	0.21	21.12	
3	zonal wind (surface)	0.5436	0.03	52.56	
4	zonal wind (500 hPa)	0.5672	0.05	53.44	
5	zonal wind (850 hPa)	0.6183	0.07	55.64	
6	air temperature	0.3362	0.10	43.32	
7	sea surface temperature (SST)	0.0013	0.40	2.64	select
8	relative humidity (up to 300 hPa)	0.1349	0.09	41.56	
9	specific humidity (up to 300 hPa)	0.1620	0.08	42.44	
10	pressure	0.3986	0.04	45.52	
11	omega (to 100 hPa)	0.6782	0.02	47.84	
12	sea level pressure (SLP)	0.0114	0.60	1.40	select
13	precipitation rate	0.4579	0.05	48.84	
14	sea precipitable water (SPW)	0.0056	0.71	1.08	select
15	momentum flux, V-component	0.5839	0.03	53.44	
16	momentum flux, U-component	0.5529	0.02	52.56	
17	zonal velocity component (surface)	0.4681	0.03	54.16	
18	zonal velocity component (500 hPa)	0.5023	0.03	51.68	
19	zonal velocity component (850 hPa)	0.5281	0.02	51.24	
20	meridional velocity component (surface)	0.6187	0.02	50.2	
21	meridional velocity component (850 hPa)	0.6747	0.04	57.4	
22	vorticity	0.2938	0.05	56.76	
24	divergence (surface)	0.5891	0.02	51.32	
23	divergence (500 hPa)	0.5992	0.03	52.2	
25	divergence (850 hPa)	0.7125	0.01	59.72	

(SPW) are selected as sea level change predictors from among 25 climatic variables simulated by CGCM3. These variables are used as DWNN and DWANFIS simulation model inputs.

3.2.1. The Discrete Wavelet artificial Neural Network model

When applying the DWNN model, the predictors and sea level time series are first decomposed to high-pass and low-pass series using three discrete wavelet functions named Haar, Db2 and Coif1. 80% (1012 series) of the 1265 series of decomposed values of predictors and predictands are used randomly to train the ANN model, while the remaining 253 series are used for model validation. The data in the calibration and validation groups are selected randomly. The ANN model includes one hidden layer

and has four and one neurons in the input and output layers respectively. The transit functions of the input, hidden and output layers are determined to be tansig, logsig and pureline respectively. Following Liang et al. (2008), the number of neurons in the hidden (NNH) layer is calculated as follows:

$$\text{NNH} = \frac{\text{NNI} + \text{NNO}}{2}, \tag{25}$$

where NNI and NNO are the numbers of neurons in the input and output layers respectively. From this equation the number of neurons in the hidden layer is determined as 2.5. However, to assess the best performance of the ANN model, ANN models, with 2, 3 and 4 neurons in the hidden layer, are considered. The results are given in Table 5. With respect to this table, the number of neurons in the hidden layer is taken to be 3, which yields the smallest RMSE value.

Table 5. Evaluation of ANN model performance using different neurons in the hidden layer

Number of neurons in the hidden layer	R	R_{NS}^2	RMSE
4	0.67	0.61	0.127
3	0.70	0.68	0.104
2	0.61	0.54	0.143

The sea level time series simulated by the DWNN model using different wavelet functions as well as the sea level time series are given in Figure 4. This shows that the model outputs are well matched with the observed values and that the worst case is when the Haar wavelet function is used. In this case the correlation between the observed and simulated values is 0.6, whereas in other cases this correlation is about 0.7. The model performance indices are given in Table 6 separately for the calibration and validation periods. This table also gives the results of the application of the individual ANN model. The results indicate a significant improvement in ANN model performance when the hybrid form of the ANN model is used, even in the worst case. Even though the performance of the DWNN models that use Db2 and Coif1 are similar, the model with the Coif1 wavelet function is selected as the best DWNN model for future sea level projection under climate change impacts because of its better performance in the calibration period.
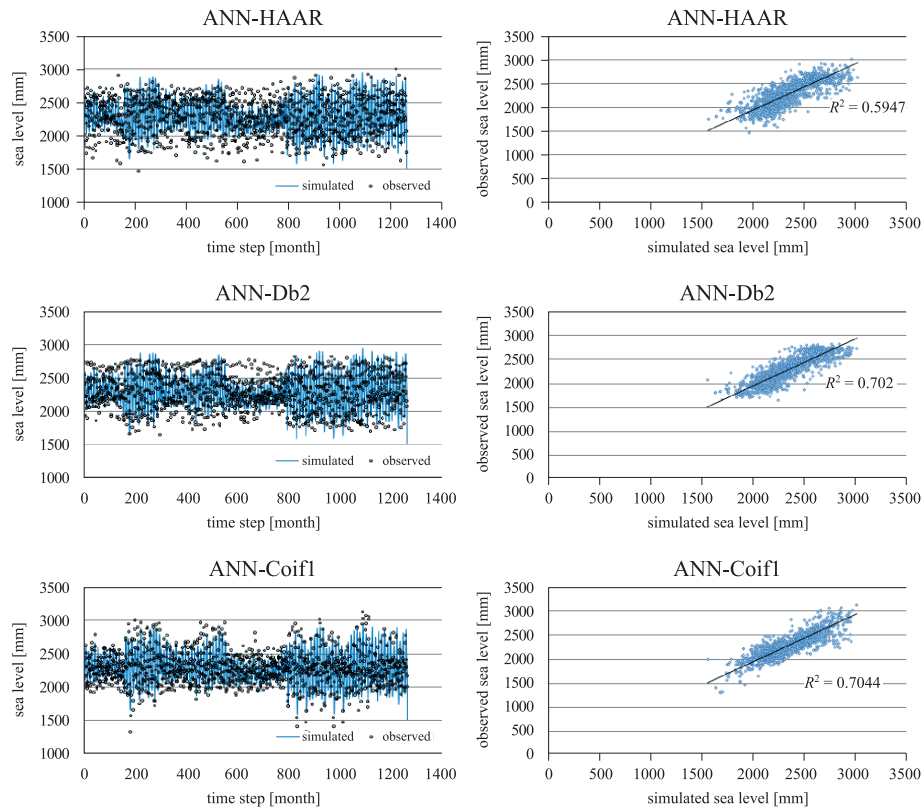
Figure 4. Comparison of the results of sea level simulation using DWNN and the observed data during the calibration and validation periods

Table 6. Performance of the proposed DWNN models for sea level prediction in the calibration and validation period

Wavelet function	Structure	Calibration			Validation		
		R	R^2_{NS}	RMSE	R	R^2_{NS}	RMSE
Haar	4-3-1	0.59	0.57	0.1327	0.56	0.53	0.1658
Db2	4-3-1	0.70	0.67	0.1179	0.67	0.64	0.1547
Coif1	4-3-1	0.70	0.68	0.1043	0.68	0.64	0.1586
without wavelet	4-3-1	0.30	0.25	0.1953	0.19	0.11	0.2517

3.2.2. The Discrete Wavelet Adaptive Neuro-Fuzzy Inference System model

As the second sea level prediction model, the pre-processed data (by wavelet transform) are used as the input of the ANFIS model. The

calibration parameters of the DWANFIS model include the number of membership functions (MF), type of membership function, number of decomposition levels and mother wavelet type. These parameters are calibrated by the available data using different wavelet transform functions.

For the development of the DWANFIS model the trimf, trapmf, gbellmf, gaussmf, gauss2mf, pimf, dsigmf and psigmf membership functions are considered. In this study, gausmf-2 is selected as the best membership function as it results in a minimum RMSE during the model training. Three membership functions are considered for each predictor. The best number of model training epochs is determined by trial and error as 20.

The sea level time series simulated by the DWANFIS model using different wavelet functions as well as historical sea level time series are shown in Figure 5. Based on this figure, the model outputs match the observed values well. The weakest result corresponds to the DWANFIS model using the Haar wavelet function and the grid partition method for ANFIS model development. In this case, the correlation of the observed and simulated values (the average of the validation and calibration periods) is 0.7, which is just about the best result obtained with the DWNN model. The model performance indices are given in Table 7 separately for the calibration and validation periods. This table also lists the results of application of ANFIS without wavelet transform, which shows a significant improvement in model performance using wavelet transformation. Furthermore, the models that use the sub-clustering method perform much better than those using the grid partitioning method. Table 7 shows that the models' performances are similar to each other as far as the application of grid partitioning is concerned, but in the DWANFIS models, which use sub-clustering, the Coif1 wavelet transform is less accurate than the other two wavelets considered. Even the DWANFIS model that uses sub-clustering and the Haar wavelet performs best for simulating the sea level on the southern coast of Iran. This is corroborated by the very similar results of the DWANFIS models developed using sub-clustering and two other types of wavelets. All of the three DWANFIS models developed using the sub-clustering method are considered for the future projection of sea level under climate change impacts.

To evaluate the performance of the model in dealing with the data through climate change simulation, the simulations of the CGCM3 model under climate change scenario A2 for the historical period (from 1990 to 2008) are used in the Anfis-Sub-Clustering-Haar simulation model. The results are given in Figure 6. This shows that the assumptions in climate change scenario development have caused the data diversity to increase somewhat.
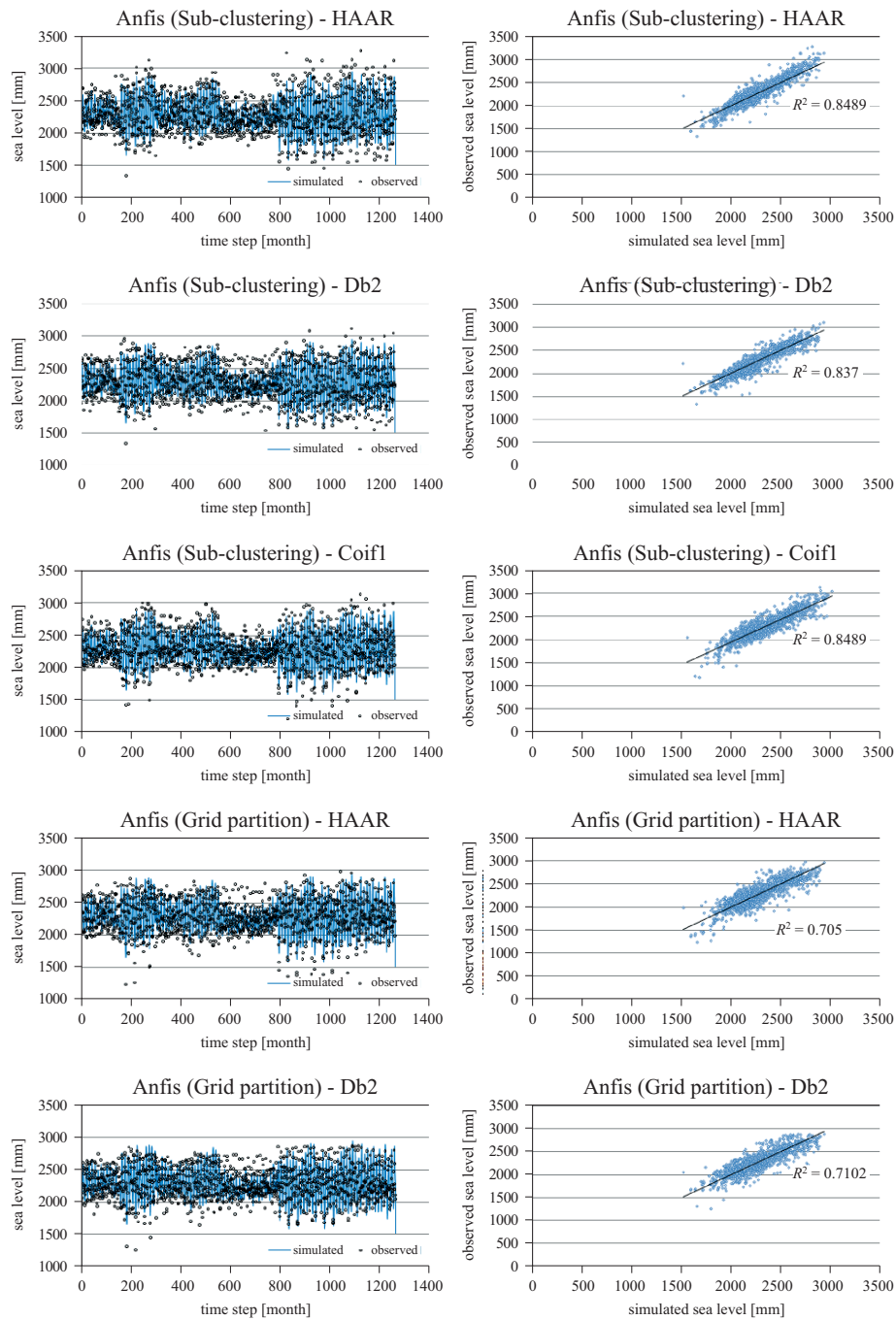
Figure 5. Comparison of the results of sea level simulation using DWANFIS and the observed data during the calibration and validation periods
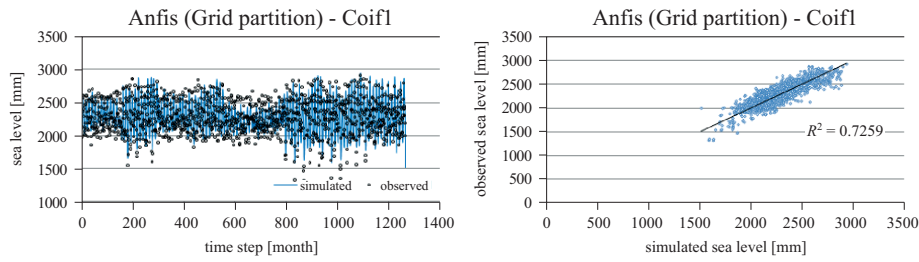
Figure 5. (*continued*)

Table 7. Performance of the proposed DWANFIS models for sea level prediction in the calibration and validation periods

| Wavelet function	ANFIS method	Calibration			Validation		
		R	R^2_{NS}	RMSE	R	R^2_{NS}	RMSE
Haar	sub-clustering	0.81	0.77	0.0885	0.85	0.80	0.0373
Db2		0.80	0.77	0.1036	0.84	0.80	0.0573
Coif1		0.74	0.70	0.1073	0.80	0.74	0. 0854
without wavelet		0.29	0.18	0.3428	0.18	0.13	0.4173
Haar	grid partition	0.67	0.64	0.1321	0.71	0.66	0.1092
Db2		0.68	0.66	0.1304	0.71	0.70	0.0968
Coif1		0.69	0.67	0.1169	0.73	0.71	0.0901
without wavelet		0.33	0.28	0.1889	0.21	0.15	0.2563
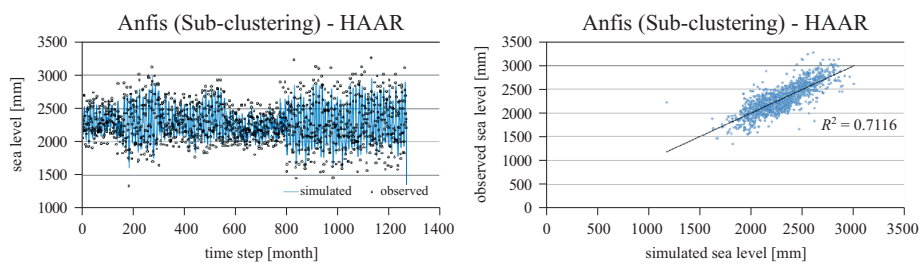
Figure 6. The performance of the selected sea level simulation model for the period 1990–2008 using the simulated climate variables from the CGCM3 model under climate change scenario A2

Table 8. Projections of sea level changes on the southern coast of Iran as a result of climate change impact for the period 2000–2100

Station name	Climate change scenario	Wavelet type	Sea level rise by 2100 [cm]
Imam Hassan	CGCM3A1b	Haar	48
		Db2	36
		Coif1	36
	CGCM3A2	Haar	72
		Db2	72
		Coif1	72
Kangan	CGCM3A1b	Haar	36
		Db2	24
		Coif1	60
	CGCM3A2	Haar	60
		Db2	72
		Coif1	72
Shahid Rajaie	CGCM3A1b	Haar	24
		Db2	12
		Coif1	48
	CGCM3A2	Haar	48
		Db2	48
		Coif1	60
Chabahar	CGCM3A1b	Haar	24
		Db2	24
		Coif1	48
	CGCM3A2	Haar	48
		Db2	48
		Coif1	60
Karachi	CGCM3A1b	Haar	6
		Db2	36
		Coif1	60
	CGCM3A2	Haar	12
		Db2	60
		Coif1	72

3.3. Projection of future sea level

The CGCM3 simulated climatic variables under the two climate change scenarios A1b and A2 are fed into the DWANFIS sea level simulation model, which has the best performance in comparison with the other models, in order to evaluate climate change impacts on sea level changes in the study region over the period 2000–2100. The Shahid Rajaie station shows the maximum changes in mean sea level during the next 100 years. The projected sea levels at all the stations for the two climate change scenarios for the period 2000–2100 using the models are presented in Table 8. The sea level changes under scenario A2 are more significant than those predicted by scenario A1b. The results of different models employed at different stations show a wide range of sea level changes at different stations, varying from 0.12 m at Shahid Rajaie station to 0.72 m at Imam Hassan, Kangan and Karachi. The results indicate that on moving eastwards along the Iranian south coast, the impacts of climate change on average sea level change decreases. The maximum average sea level rise is projected at the Imam Hassan station and the lowest value corresponds to the Shahid Rajaie station.

The models developed in this study are based on a limited length time series of sea level data, so supplying more data would increase the reliability of the models and results. However, just a projection of future sea level changes is given here; for real case applications, further studies will be needed, especially on data and model uncertainty. The uncertainties in the selection of different climate change scenarios and GCM models are not considered. The models employed do not incorporate uncertainties, which could play an important role in the evaluation of climate change impacts. Different types of ANN models can also be incorporated in the development of the DWNN model to improve its performance. Furthermore, the application of different methods involving data sharing and overlapping in different series for predictor selection can provide useful information.

4. Summary and conclusion

Precise sea level projections are important for coastal navigation and offshore engineering applications as well as for marine recreational activities, especially for development programmes in coastal regions. This study proposes a methodology for projecting climate change impacts on sea level rise. This methodology uses stepwise regression to select the most appropriate predictors and then employs hybrids of ANN and ANFIS with wavelet transformation (named DWNN and DWANFIS respectively) for sea level simulation. The wavelet transform decomposes the predictor

and predictand time series into smoother time series to be used in the simulation models. The decomposed time series of predictors are fed into the ANN/ANFIS models individually to simulate decomposed time series of sea level. The outputs of these models are composed to form the simulated sea level time series. The proposed method is to be employed on the southern coast of Iran. The set of sea level predictors in this region includes Sea Level Pressure (SLP), Geopotential Height (GH), Sea Surface Temperature (SST) and Sea Precipitable Water (SPW). The results show that the DWANFIS model performs better than the DWNN model in sea level simulation. This study shows that the average sea level rise at the study region is about 0.33 m and 0.59 m under climate change scenarios of A1b and A2 respectively. Considerable expanses of flat coastal areas will be inundated as a result of sea level increase. This range of sea level change would result in substantial changes in coastal ecosystems and would give rise to significant economic problems.

References

Adamowski J., 2008a, *Development of a short-term river flood forecasting method for snowmelt driven floods based on wavelet and cross-wavelet analysis*, J. Hydrol., 353 (3–4), 247–266, http://dx.doi.org/10.1016/j.jhydrol.2008.02.013.

Adamowski J., 2008b, *River flow forecasting using wavelet and cross-wavelet transform models*, Hydrol. Proc., 22 (25), 4877–4891, http://dx.doi.org/10.1002/hyp.7107.

Anctil F., Tape G. D., 2004, *An exploration of artificial neural network rainfall runoff forecasting combined with wavelet decomposition*, J. Environ. Eng. Sci., 3 (S), 121–128, http://dx.doi.org/10.1139/s03-071.

Barford L. A., Fazzio R. S., Smith D. R., 1992, *An introduction to wavelets*, Hewlett-Packard Lab., HPL-92-124, 27 pp.

Bindoff N. L., Willebrand J., Artale, V., Cazenave A., Gregory J., Gulev S., Hanawa K., Le Quere C., Levitus S., Nojiri Y., Shum C. K., Talley L. D., Unnikrishnan A. S., 2007, *Observations: oceanic climate change and sea level*, [in:] *Climate change 2007: the physical science basis*, Contribution of Working Group I to the Fourth Assessment Report of the Intergovernmental Panel on Climate Change, Solomon S., Qin D., Manning M., Chen Z., Marquis M., Averyt K. B., Tignor M. & Miller H. L. (eds.), Cambridge Univ. Press, Cambridge, New York, 387–429.

Burn D. H., Cunderlik J. M., 2004, *Hydrological trends and variability in the Laird River basin*, Hydrol. Sci. J., 49 (1), 53–67, http://dx.doi.org/10.1623/hysj.49.1.53.53994.

Cannas B., Fanni A., See L., Sias G., 2006, *Data preprocessing for river flow forecasting using neural networks: wavelet transforms and data partitioning*,

Phys. Chem. Earth, 31 (18), 1164–1171, http://dx.doi.org/10.1016/j.pce.2006.03.020.

Chiu S. L., 1994, *Fuzzy model identification based on cluster estimation*, J. Int. Fuzzy Syst., 2, 267–278.

Coulibaly P., Burn D. H., 2005, *Spatial and temporal variability of Canadian seasonal streamflows*, J. Climate, 18 (1), 191–210, http://dx.doi.org/10.1175/JCLI-3258.1.

Drago A. F., Boxall S. R., 2002, *Use of the wavelet transform on hydro-meteorological data*, Phys. Chem. Earth, 27 (32–34), 1387–1399, http://dx.doi.org/10.1016/S1474-7065(02)00076-1.

Gilbert R. O., 1987, *Statistical methods for environmental pollution monitoring*, Van Nostrand Reinhold, New York, 320 pp.

Haykin S., 1998, *Neural networks – a comprehensive foundation*, 2nd edn., Prentice-Hall, Upper Saddle River, NJ, 26–32.

Houghton J. T., Ding Y., Griggs D. J., Noguer M., van der Linden P. J., Xiaosu D. (eds.), 2001, *Climate change 2001: The scientific basis*, Contribution of Working Group I to the Third Assessment Report of the Intergovernmental Panel on Climate Change, Cambridge Univ. Press, Cambridge, New York, 639–693.

Intergovernmental Panel on Climate Change (IPCC), 2007, *Climate change 2007: impact, adaptation and vulnerability. Contribution of Working Group II to the Fourth Assessment Report of the IPCC*, Cambridge Univ. Press, Cambridge, 976 pp.

Jang J. S. R., 1993, *ANFIS: adaptive network-based fuzzy inference system*, IEEE T. Syst. Man Cyb., 23 (3), 665–685, http://dx.doi.org/10.1109/21.256541.

Kendall M. G., 1975, *Rank correlation methods*, Charles Griffin, London, 202 pp.

Kim T. W., Valdés J. B., 2003, *Nonlinear model for drought forecasting based on a conjunction of wavelet transforms and neural networks*, J. Hydrol. Engin., 8 (6), 319–328, http://dx.doi.org/10.1061/(ASCE)1084-0699(2003)8:6(319).

Kleinow T., 2002, *Testing continuous time models in financial markets*, Ph. D. thesis, Buchhändler-Vereinigung, Berlin, 244 pp.

Küçük M., 2004, *Modeling river flow series using wavelet transform*, Ph. D. thesis, Istanbul Tech. Univ., Istanbul, (in Turkish).

Labat D., 2005, *Recent advances in wavelet analyses: Part 1. A review of concepts*, J. Hydrol., 314 (1–4), 275–288, http://dx.doi.org/10.1016/j.jhydrol.2005.04.003.

Liang S. X., Li M. C., Sun Z. C., 2008, *Prediction models for tidal level including strong meteorologic effects using a neural network*, Ocean Eng., 35 (7), 666–675, http://dx.doi.org/10.1016/j.oceaneng.2007.12.006.

Long C. J., Datta S., 1996, *Wavelet based feature extraction for phoneme recognition*, Proc. 4th Int. Conf. Spoken Lang. Process., 1, 264–267.

Lu R. Y., 2002, *Decomposition of interdecadal and interannual components for North China rainfall in rainy season*, Chinese J. Atmos., 26, 611–624, (in Chinese).

Maguire L. P., Roche B., McGinnity T. T., McDaid L. J., 1998, *Predicting a chaotic time series using a fuzzy neural network*, Inform. Sci., 112 (1–4), 125–136, http://dx.doi.org/10.1016/S0020-0255(98)10026-9.

Makarynskyy O., Makarynska D., Kuhn M., Featherstone W. E., 2004, *Predicting sea level variations with artificial neural networks at Hillarys Boat Harbour, Western Australia*, Estuar. Coast. Shelf Sci., 61 (2), 351–360, http://dx.doi.org/10.1016/j.ecss.2004.06.004.

Mallat S., 1998, *A wavelet tour of signal processing*, Acad. Press, San Diego, 577 pp.

Masters T., 1993, *Practical Neural Network Recipes in C++*, Acad. Press, San Diego, 493 pp.

Meyer Y., 1993, *Wavelets: algorithms and applications*, Soc. Ind. Appl. Math., Philadelphia.

Mittal A., Aadaleesan P., 2010, *A new Hammerstein model for non-linear system identification*, Int. J. Comm. Netw. Secur. (IJCNS), 1 (3), 1–12.

Nourani V., Alami M. T., Aminfar M. H., 2009, *A combined neural-wavelet model for prediction of watershed precipitation, Lighvanchai, Iran*, Eng. Appl. Artif. Intelligence, 22 (3), 466–472.

Nourani V., Kisi O., Komasi M., 2011, *Two hybrid Artificial Intelligence approaches for modeling rainfall-runoff process*, J. Hydrol., 402 (1–2), 41–59, http://dx.doi.org/10.1016/j.jhydrol.2011.03.002.

Partal T., Cigizoglu H. K., 2008, *Estimation and forecasting of daily suspended sediment data using wavelet-neural networks*, J. Hydrol., 358 (3–4), 317–331, http://dx.doi.org/10.1016/j.jhydrol.2008.06.013.

Partal T., Kişi O., 2007, *Wavelet and neuro-fuzzy conjunction model for precipitation forecasting* J. Hydrol., 342 (1–2), 199–212, http://dx.doi.org/10.1016/j.jhydrol.2007.05.026.

Partal T., Küçük M., 2006, *Long-term trend analysis using discrete wavelet components of annual precipitations measurements in Marmara region (Turkey)*, Phys. Chem. Earth, 31 (18), 1189–1200, http://dx.doi.org/10.1016/j.pce.2006.04.043.

Pfeffer W. T., Harper J. T., O'Neel S., 2008, *Kinematic constraints on glacier contributions to 21st-century sea-level rise*, Science, 321 (5894), 1340–1343, http://dx.doi.org/10.1126/science.1159099.

Rajaee T., Mirbagheri S. A., Zounemat-Kermani M., Nourani V., 2009, *Daily suspended sediment concentration simulation using ANN and neuro-fuzzy models*, Sci. Total Environ., 407 (17), 4916–4927, http://dx.doi.org/10.1016/j.scitotenv.2009.05.016.

Rumelhart D. E., Hinton G. E., Williams R. J., 1986, *Learning representations by back-propagating errors*, Nature, 323, 533–536, http://dx.doi.org/10.1038/323533a0.

Salahshoor K., Kordestani M., Khoshro S., 2010, *Fault detection and diagnosis of an industrial steam turbine using fusion of SVM (support vector machine) and ANFIS (adaptive neuro-fuzzy inference system) classifiers*, Energy, 35 (12), 5472–5482, http://dx.doi.org/10.1016/j.energy.2010.06.001.

Wang D., Ding J., 2003, *Wavelet network model and its application to the prediction of hydrology*, Nature Sci., 1 (1), 67–71.

Xingang D., Ping W., Jifan C., 2003, *Multi-scale characteristics of the rainy season rainfall and interdecadal decaying of summer monsoon in North China*, Chinese Sci. Bull., 48 (24), 2730–2734.

Zwiers F. W., Storch H. V., 2003, *Statistical analysis in climate research*, Cambridge Univ. Press, Cambridge, 495 pp.